

APPARATUS AND COMPUTER X-RAY TOMOGRAPHY: VISUALIZATION OF INTRINSIC STRUCTURE, EVALUATION OF PERFORMANCE AND LIMITATIONS

Marina Chukalina
Sergey Zaitsev
Maxim Knyazev
C. J. Vanegas
Institute of Microelectronics
Technology RAS
142432 Chernogolovka
Moscow District, Russia
marina@ipmt-hpm.ac.ru
zaitsev@ipmt-hpm.ac.ru

Dmitry Nikolaev

Institute for Information
Transmission Problems, RAS
Bol'shoj Karetnyj lane, 19
101447, Moscow, Russia
dimonstr@iitp.ru

Alexandre Simionovici

Laboratoire des Sciences
de la Terre
ENS, 46 allée d'Italie
Lyon, 69007 Lyon, France
asimiono@ens-lyon.fr

KEYWORDS

Confocal apparatus and computer tomography in medicine, image visualization, dose deposition.

ABSTRACT

In this paper we compare confocal apparatus tomography and computer tomography for medical use. Two aspects are illustrated: the process of image visualization and the dose deposition. The latter aspect is a damage factor of the object under investigation; it is why the data collection time is evaluated. Two principal tomography schemes are described and the expressions connecting the collected signal value with the object's internal structure are given. Based on the expression, the process of image visualization is described and the dose deposition is calculated for both cases. The object's classification is introduced to choose the optimal experimental scheme for the object under study.

INTRODUCTION

The use of X-ray microdiagnostic systems in biology and medicine has grown, covering such areas of investigations as the tomography of small animals (Asadchikov et al. 2004), the tomography of labeled cells (Schneider et al. 2001), the three-dimensional evaluation of biocompatible materials (Muller et al. 2001), the microtomography for the analysis of osteointegration around implants (Bernhardt et al. 2004) etc. Fluorescence microtomography combines fluorescence analysis with X-ray tomographic techniques and enables multielemental observation (Golosio et al. 2003).

The terms "apparatus" and "computer" describe two modes of the fluorescence collection during the experiment. In the first case a parallel (Takeda et al. 1995) or a confocal (Zaitsev et al. 2002) collimator is

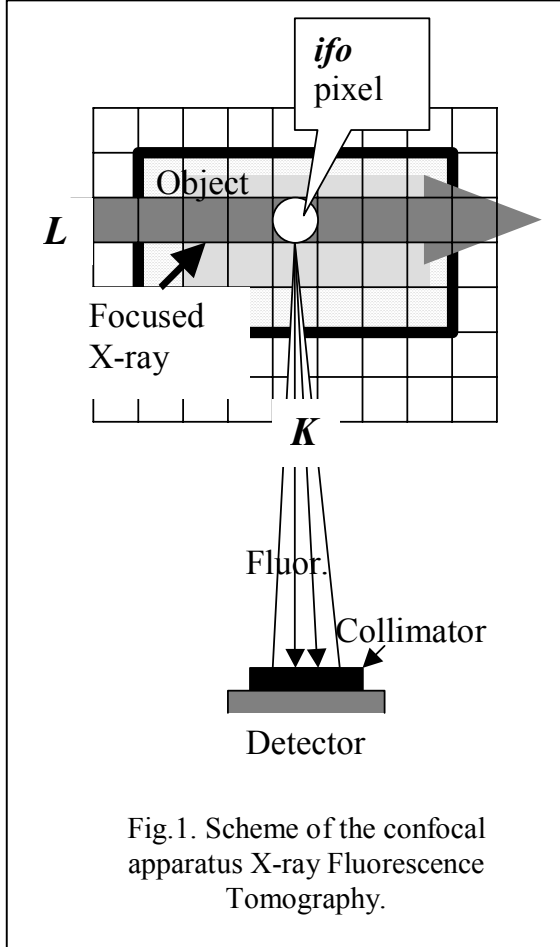
placed in front of the energy-dispersive detector window to decrease the detector solid angle and to localize the fluorescence generation zone from where the signal is collected. The registered signal is a function of the detector focal spot position. In the second case there is no space localization. The experimental set-up repeats the X-ray computer tomography parallel scheme but the fluorescence is registered in addition to the absorption signal. The registered signal is now a function of the X-ray microbeam position and the rotation angle (Simionovici et al. 1999). To compare the advantages and limitations of apparatus tomography and computer tomography we have analysed the image visualization process. The data manipulation procedures and the signal collection time (radiation dose) are evaluated for both cases.

CONFOCAL APPARATUS TOMOGRAPHY WITH X-RAY MICROBEAM

The scheme for confocal apparatus X-ray fluorescence tomography is presented in Fig.1. An X-ray microfocus beam (Snigireva et al. 2003) illuminates a small volume of the sample. That part of the sample generates fluorescence which is collected by an energy-dispersive detector through the confocal collimator (Fig. 2) placed in front of the detector. The collimator (Fig.2) manufactured by Microelectronics Technology (Zaitsev et al. 2004) features a microfocus spot size. The intersection of the microbeam and the collimator focus localizes a zone from where the fluorescence is collected. The sample mounted on the sample-stage is translated in X-Y-Z directions with an applicable offset. Lateral resolution of the technique is determined by the scanning step, the X-ray beam size and the collimator focal spot size, appropriately. Usually the scanning step is equal to the collimator focus size and a

pixel has the same size (Fig.1). Below we consider pixels rather than voxels to simplify the considerations. For each "focal pixel" (*ifo* pixel on Fig.1) a fluorescence spectrum is registered. Each spectrum is mathematically processed to obtain a discrete set of values.

The spectrum is mathematically processed to obtain a discrete set of values, and the value given to this pixel is the number of one of the fluorescence lines. Let us say that M elements (M fluorescence lines) are measured and N^2-1 sample translations are made during an experiment. The image size is N by N pixels. Each image corresponds to one element. But the image



is not the distribution of the element until an additional process including an attenuation correction has been done. To describe the correction needed to visualize the real image of the i th element distribution, the mathematical model of the signal S_{ifo}^i should be written

$$S_{ifo}^i = I_0 C_{ifo}^i \mu^i \Delta \eta^i \Phi_{ifo}^i \sum_{j=1}^J F_{ifo}^{ij} \quad (1)$$

Here I_0 is the flux of the X-ray beam, C_{ifo}^i is the i th element concentration, μ^i is the linear attenuation coefficient of the X-ray by i th element, Δ is the linear size of the pixel, η^i is the fluorescence yield of i th element line, J is the number of collimator pinholes.

$$\Phi_{ifo}^i = \exp\left(-\sum_{k=0}^{K-1} \mu[ifo - K + k] \Delta\right) \quad (2)$$

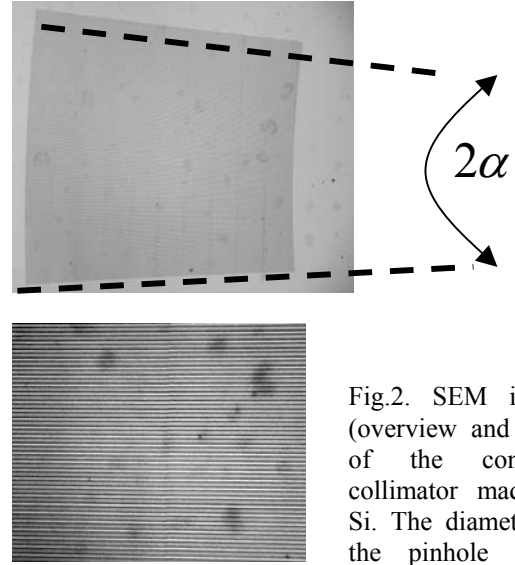


Fig.2. SEM image (overview and part) of the confocal collimator made in Si. The diameter of the pinhole is 2 microns, the number of pinholes is 200, the length of the pinhole is 1 mm, the focal distance is 5 mm.

Here $\mu[ifo] = \sum_{i=1}^M C_{ifo}^i \mu^i$. Φ_{ifo}^i describes the X-ray attenuation of the X-ray by the sample along the X-ray's path (Fig.1). To calculate it for all pixels to the left of *ifo* pixel, the element concentrations should be known. This shows that the scanning procedure should be started from the left.

$$F_{ifo}^{ij} = \int_{\Omega_{pin}} d\Omega \exp\left(-\sum_{l=1}^{l-1} v^l [ifo - lN - \text{int}(\Delta l \alpha_j(\Omega))] \Delta\right) \quad (3)$$

Here j is the collimator pinhole number (Fig.2), $v^i[ifo] = \sum_{j=1}^M C_{ifo}^i v_j^i$ is the linear attenuation coefficient of

the i th fluorescence line by the sample, Ω_{pin} is the solid angle of the collimator pinhole (Fig.2),

$$\alpha_j = -\alpha + \frac{2\alpha}{N_{pin} - 1} (j - 1)$$

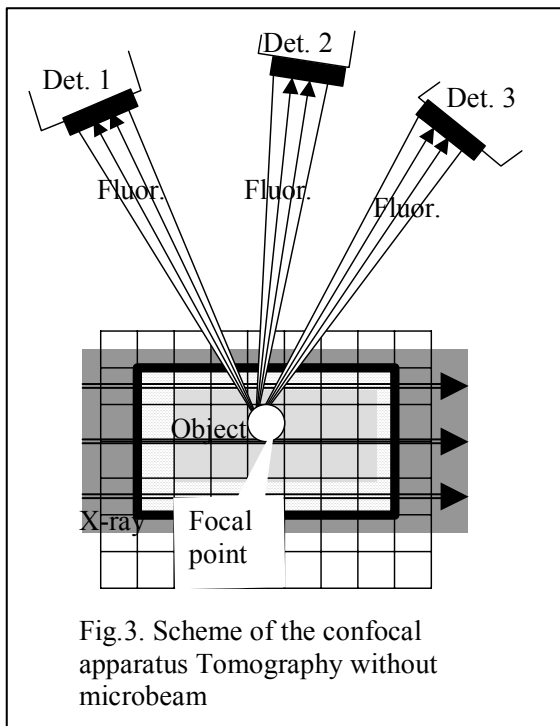
is the axis of the j th

pinhole position. F_{ifo}^{ij} describes the attenuation of the i th fluorescence line by the sample on the route to the detector (Fig.1). To calculate the corresponding values it is necessary to know the elements concentrations of the pixels laying on the fluorescence way. In Fig.1 it is seen that that the scanning procedure should be organized from bottom to top. The numbering of the pixels in Fig.1 corresponds to the scanning procedure. The first pixel is the bottom left pixel and the last pixel is the top right pixel.

Now it is possible to write the algorithm for the image visualization by confocal apparatus tomography Fig.1. To start with it is necessary to organize the links to the tables containing the required linear attenuation coefficients of the M elements for the X-ray and all fluorescence lines; then to start the tour over the pixels according to the scanning scheme; for each pixel measured spectrum to describe to the vector with M components; to calculate $\Phi_{if_0}^i$ and $F_{if_0}^{ij}$ for all collimator pinholes; to calculate $C_{if_0}^i$ and to move to the next pixel. The procedure of the image visualization can be performed in-situ (pixel by pixel). It is very important because the data collection time (dose deposition) can be varied from pixel to pixel to achieve the required density resolution.

CONFOCAL APPARATUS TOMOGRAPHY WITHOUT X-RAY MICROBEAM

Despite very promising prospects, to organize the intersection of the X-ray microbeam and the collimator microfocus is a very difficult task. The first experiment without X-ray microbeam was carried out on February 2005 at the ESRF (Zaitsev et al. 2005). The scheme of the data collection is presented in Fig. 3.



Simulation results are presented in Fig.4. Parameters for the simulation: the sample is 5 microns' thickness Al strip in PMMA, X-ray beam energy is 10 keV, no backscattering effects are taking into account. The scanning procedure is the same as the procedure described above (Fig.1). The apparatus function of three collimators system is not so simple as in the previous case, however, we can calculate it before the

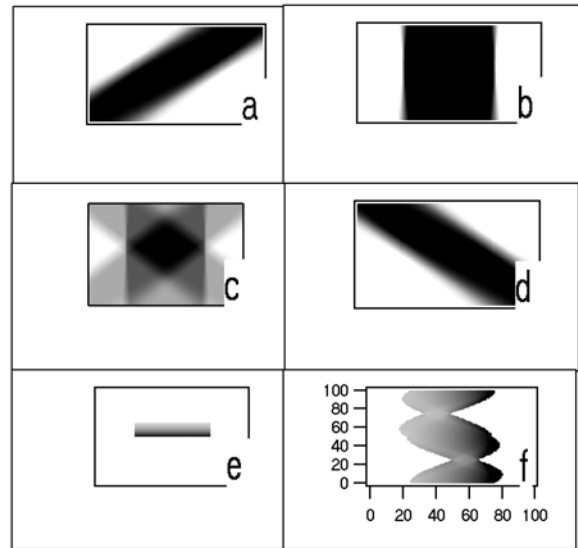


Fig.4. Simulation results. Signals collected with the different tomography set-ups. a) Signal from Det. 3 (Fig.3); b) Signal from Det.2 (Fig.3); c) Sum of Signals a,b,d ; d) Signal from Det.1. (Fig.3); e) Signal collected on Fig.1; f) Set of Projections (Fig.5).

experiment. The registered signal is the convolution of the AI image, which we are interested in visualizing, with the apparatus function. After the implementation of the deconvolution procedure it will be possible to see the result of the AI strip visualization. This result cannot give quantitative information about the sample (if attenuation is not negligible) but the boundaries of the object will be found. And again the data collection time from pixel to pixel is controlled and can be varied.

COMPUTER X-RAY FLUORESCENCE TOMOGRAPHY

The last scheme is the computer tomography scheme. The sample is mounted on the sample stage which is moved in X-Z directions and is rotated with some angle step over 360° . For X-ray fluorescence tomography it is important to have the total angle because the attenuation effects for the characteristic lines are different for and rotation angles if the sample is not homogeneous and has no central symmetry. The detector collects all quanta generated on the route of the X-ray beam grabbing by the detector's solid angle. The registered signal now is a function of the X-ray microbeam position and the rotation angle (Fig.4f). The Y-direction on the image is the rotation angle axis and X-direction is the microbeam position axis). For the image visualization it is necessary to move from the signal space to the image space. Write the mathematical model of the signal formation

$$S^i(\rho, \varphi) = \Omega_{\text{det}} I_0 \mu^i \eta^i \int_{L_1} C^i(l) \Phi(l) F^i(l) dl \quad (4).$$

L_1 is the direction of the X-ray microbeam (contrary to the y' -axis direction (Fig.5)) and Ω_{det} is the detector's solid angle.

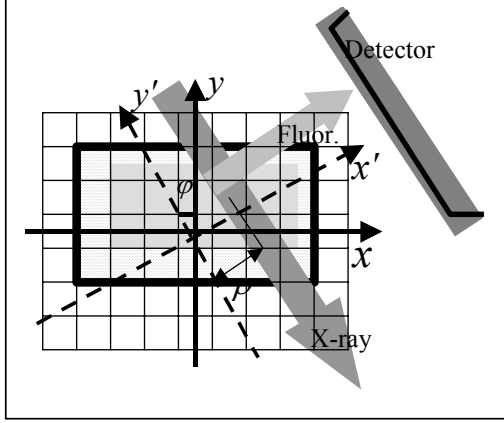


Fig.5. Scheme of the Computer Tomography. The microbeam position is described by ρ . ϕ is the rotation angle.

Let us suppose N translation steps and N rotations are done during the experiment. Then N^2 spectra are collected and each spectrum is transformed to the M -component vector. The modified algebraic technique (Chukalina et al. 2002) is used to visualize M images. The integral equation (4) is presented by the nonlinear algebraic system which is solved by Kaczmarz method.

DOSE DEPOSITION

Let us try to answer the question – how many incident photons TI_0 (here T is the data collection time) are needed to resolve a fractional element concentration fluctuation $\Delta(x, y, elem) = \frac{C_{min}(x, y)}{C_{max}(x, y)}$.

To answer this question let us introduce the other value $\delta = \frac{\sqrt{I}}{I}$. Here I is the number of quanta collected by

the detector (from one pixel in the apparatus case and for one microbeam position in computer one). For computer tomography if N translations and N rotation are done during experiment, then the total time for the computed tomography is equal

$$T_{total}^{comput} = \frac{\Phi}{\delta^2} \frac{1}{\Omega_{det}} \frac{1}{C_{min}} N^2 \quad (5)$$

Now Φ includes all attenuation terms. The situation is not the same for apparatus tomography, where it is possible to control the number of quanta coming from each pixel. The data collection time can be varied in agreement with the concentration fluctuations. Then for the pixels with the C_{min} concentration value the data collection time is equal to:

$$T_{min} = \frac{\Phi}{\delta^2} \frac{1}{\Omega_{pin} J} \frac{1}{C_{min}}$$

and for the pixels with the C_{max} concentration value it is equal to:

$$T_{max} = \frac{\Phi}{\delta^2} \frac{1}{\Omega_{pin} J} \frac{1}{C_{max}} = \frac{\Phi}{\delta^2} \frac{1}{\Omega_{pin} J} \frac{\Delta}{C_{min}}$$

Let us introduce the value N^{min} which is the number of pixels with the C_{min} concentration value. Then the number of pixels with concentration C_{max} is $N^2 - N^{min}$ and the total time for the apparatus tomography can be calculated by

$$T_{total}^{app} = T_{min} N^{min} + T_{max} (N^2 - N^{min}) = \frac{\Phi}{\delta^2} \frac{1}{\Omega_{pin} J} \frac{1}{C_{min}} (N^{min} + \Delta [N^2 - N^{min}]) \quad (6)$$

Now we can compare the two tomography experiments (computed and apparatus) from the data collection time point of view:

$$\frac{T_{total}^{comp}}{T_{total}^{app}} = \frac{N^2}{N^{min} + \Delta [N^2 - N^{min}]} \frac{\Omega_{pin} J}{\Omega_{det}} \quad (7)$$

and can analyse the conditions when one or the other technique will be preferable.

OPTIMAL CONDITIONS FOR SCHEME CHOICE

Let us consider three models of the sample description. The first model is built on the hypothesis that $\Delta \rightarrow 1$. There is a very small variation between concentrations from pixel to pixel. Then

$$\frac{N^2}{N^{min} + \Delta [N^2 - N^{min}]} \approx 1$$

and now we rewrite Expression (7)

$$\frac{T_{total}^{comp}}{T_{total}^{app}} \approx \frac{\Omega_{pin} J}{\Omega_{det}} \quad (8)$$

Let us make an estimation of this ratio based on Fig.1. The solid angle of a detector placed at 5 cm distance

from a sample is $\Omega_{det} = \frac{r_{det}^2}{R^2} = 0.01$. The surface of the detector window is 25 mm². The diameter of the collimator channel is about 2 μ m. Solid angle of the

channel is $\Omega^{col} = \frac{\pi r_{channel}^2}{R^2} = 5 \times 10^{-11}$ Compact packing of the channels by microelectronics techniques (Zaitsev et al. 2004) on a 25 mm² square chip allows the

placing of 10^8 channels. We have $\frac{T_{total}^{comp}}{T_{total}^{app}} \approx 0,5$ which

means that the time needed to make the apparatus tomography experiment is twice as much as the computed tomography time.

The second model describes the situation when $\Delta = \frac{1}{2}$.

Then we rewrite Expression (7) in agreement with the model

$$\frac{N^2}{N^{\min} + \Delta[N^2 - N^{\min}]} = \frac{2N^2}{N^2 + N^{\min}}$$

and consider two extreme cases $N^{\min} \rightarrow 0$ and $N^{\min} \rightarrow N^2$. The expression (8) is rewritten as

$$\frac{1}{2} < \frac{T_{total}^{comp}}{T_{total}^{appar}} < 1$$

and the times for both cases start to

be commensurable.

The last model is based on the condition $\Delta \rightarrow 0$. Then expression (7) is modified to

$$\frac{N^2}{N^{\min} + \Delta[N^2 - N^{\min}]} \approx \frac{N^2}{N^{\min}}$$

and the comparison of the data collection times is described by:

$$\frac{T_{total}^{comp}}{T_{total}^{app}} \approx \frac{\Omega_{pin} J}{\Omega_{det}} \frac{N^2}{N^{\min}}$$

This result shows that if $\Delta \rightarrow 0$ (a sample has regions with very low concentration ratios of an element) then apparatus tomography has big advantages versus the computed one.

CONCLUSION

In this paper confocal apparatus tomography and computer tomography are compared from an image visualization point of view. The image visualization procedure is faster and simpler for the apparatus case, however, an additional parameter (dose deposition) should be taken into account if the tomography is used in medicine. It was shown that the data collection time (or dose deposition) depends on the sample type. As a conclusion, it should be mentioned that the sequential application of both techniques can give additional advantages. The computed tomography implemented with a 'big' scanning step size and a 'big' rotation angle value gives a preliminary picture about the sample volume and then using apparatus tomography it is possible to investigate the chosen small volumes with a good lateral resolution and good sensitivity. Confocal apparatus tomography has the extra advantage of being able to perform "partial volume tomography" that is analyzing a small volume inside a bigger one, by partial scanning.

This work was partly financially supported by the NATO Scientific Affairs Division through grant nr. EST-CLG-979530, by the PICS 22-10 and RFBR Programs for scientific investigations. In addition the work of Dr. M. Chukalina was partly supported by the Institute of Crystallography RAS, Russia .

REFERENCES

Asadchikov, V., A. Buzmakov, Yu. Zanevskii, V. Zryuev, R. Senin, S. Saveliev, L. Smikov, D. Tudosy, G.

- Cheremuhina, E. Cheremuhin, S. Chernenko and A. Chulichkov. 2004. "X-ray transmission tomography with 0.7-1.54 Å in laboratory conditions". In *Proceedings of X-ray Optics Workshop* (Nizhny Novgorod, May 2-7). IPM RAS, 123-130.
- Bernhardt, R., D. Scharnweber, B. Müller, P. Thurner, H. Schliephake, P. Wyss, F. Beckmann, J. Goebbels and H. Worch. 2004. "Comparison of microfocus and synchrotron X-ray tomography for the analysis of osteointegration around Ti6Al4V-implantants". *European Cells and Materials* 7, 42-51.
- Chukalina, M, A. Simionovici, A. Snigirev and T. Jeffries. 2002. "Quantitative characterization of microsamples by X-ray Fluorescence Tomography" *X-Ray spectroscopy* 31, No. 6, 448-450.
- Golosio, B., A. Simionovici, A. Somogyi, L. Lemelle, M. Chukalina and A. Brunetti. "Internal elemental microanalysis combining X-ray fluorescence, Compton and transmission tomography". 2003. *Journal of Applied Physics* 94, No. 1, 145-156.
- Müller, B, P. Thurner, F. Beckmann, T. Weitkamp, C. Rau, R. Bernhardt, E. Karamuk, L. Eckert, S. Buchloh, E. Wintermantel, D. Scharnweber and H. Worch. 2001. "Non-destructive three-dimensional evaluation of biocompatible materials by microtomography using synchrotron radiation". In *Proceedings of the SPIE Meeting* (San Diego, Aug. 2-3), SPIE 4503, 178-188.
- Schneider, G., D. Weiss; M. A. LeGros; S. Vogt, C. Knöchel and E.H. Anderson. 2001. "Nanotomography of labeled cryogenic cells". In *Proceedings of the SPIE Meeting* (San Diego, Aug. 2-3). SPIE 4503, 156-165.
- Simionovici, A., M. Chukalina, M. Drakopoulos, I. Snigireva, A. Snigirev, Ch. Schroer, B. Lengeler and F. Adams. 1999. "X-ray fluorescence microtomography: experiment and reconstruction". *SPIE* 3772, 304-310.
- Snigireva, I., V. Yunkin, S. Kuznetsov, M. Grigoriev, M. Chukalina, L. Shabel'nikov, A. Snigirev, M. Hoffmann and E. Voges. 2003. "Focusing properties of silicon refractive lenses: comparison experimental results with the computer simulation". *SPIE* 5195, 32-39.
- Takeda, T., T. Maeda, T. Yuasa, T. Akatsuka, T. Ito, K. Kishi, J. Wu, M. Kazama, K. Hyodo and Y. Itai. 1995. "Fluorescent scanning x-ray tomography with synchrotron radiation". *Rev. Scien. Instrum.* 66, No. 2, 1471-1473.
- Zaitsev, S., M. Chukalina and P. Mastripiolito. 2002. "X-ray fluorescence diagnostics with confocal collimator for the data collecting". In *Proceeding of the Workshop on X-ray Optics*. (Nizhny Novgorod, Russia, March 14-17). IPM RAS, 293-298 (in Russian).
- Zaitsev, S., M. Knyazev, S. Dubonos, and A. Bazhenov. 2004. "Fabrication of 3D photonic structures". *Microelectronic Engineering* 73-74, 383-387.
- Zaitsev, S., M. Chukalina, A. Simionovici and E. Ziegler. 2005. "Pilot testing method of fluorescent microtomography based on confocal collimators" *Experiment at the ESRF Proposal MI724* (February 17-20).
- simulation.
al that can be found in the paper!

AUTHOR BIOGRAPHIES

MARINA V. CHUKALINA received her PhD in Physics at the Institute of Microelectronics Technology RAS where she has been working since 1988. Her

interests include the development of signal and image processing tools for X-ray Microscopy and Tomography. Her Web-page can be found at <http://www.ipmt-hpm.ac.ru/english/labs/lcd/>

SERGEY I. ZAITSEV is Dr. of Science at the Institute of Microelectronics Technology RAS, Russia. His research interests concentrate on the theory of solid state kinetics.

MAXIM KNYAZEV is PhD student at the Institute of Microelectronics Technology from 2001. His research area is microelectronics technology.

ALEXANDRE SIMIONOVICI received his PhD in nuclear physics, worked at the ESR as a beamline lider and now carries his investigations in the Laboratoire des sciences de la terre, ENS, Lyon.

DMITRY P. NIKOLAEV received PhD degree at Moscow State University in 2004 in Physics. He has been a research scientist at the Institute for Information Transmission Problems RAS since 2000. His research activities are in the areas of computer vision with primary application to colour image understanding.